Astronomy & Astrophysics manuscript no. 2014-04-04˙MIR˙HD100453˙HD34282
April 4, 2014

Large gaps in the transitional disks of HD 100453 and HD 34282

Connecting the gap size to the spectral energy distribution

S. Khalafinejad[1,2], K. M. Maaskant[2], and A.G.G.M Tielens[2]

[1] Hamburg Observatory, Hamburg University, Gojenbergsweg 112, 21029 Hamburg, Germany
[2] Leiden Observatory, Leiden University, P.O. Box 9513, 2300 RA Leiden, The Netherlands

April 4, 2014

ABSTRACT

Context. The formation of gaps in protoplanetary disks is one of the most important signposts of disk evolution and possibly the formation of planets.
Aims. We aim to characterize the 'flaring' disk structure around the Herbig Ae/Be stars HD 100453 and HD 34282. Their spectral energy distributions (SEDs) show an emission excess between $15 - 40$ μm, but very weak (HD 100453) and no (HD 34282) signs of the 10 and 20 μm amorphous silicate features. We investigate whether this implies the presence of large gaps.
Methods. Spatially resolved mid-infrared Q-band images taken with Gemini South/T-ReCS are investigated. We perform radiative transfer modeling and examine the radial distribution of dust. We simultaneously fit the Q-band images and SEDs of HD 100453 and HD 34282. Our solutions require that the inner-halos and outer-disks are separated by large dust depleted gaps.
Results. The inner edges of the outer disks of HD 100453 and HD 34282 have temperatures of $\sim$ 160 K and $\sim$ 60 K respectively. Because of the high surface brightnesses of these walls, they dominate the emission in the Q-band. Their radii are therefore well constrained at 17^{+2}_{-2} AU and 79^{+31}_{-17} AU, respectively.
Conclusions. HD 100453 and HD 34282 have large disk gaps. We find that the locations and sizes of disk gaps are connected to the SED, as traced by the mid-infrared flux ratio $F_{30}/F_{13.5}$. The absence of amorphous silicate features in the observed SEDs is caused by the depletion of small ($\lesssim 1$ μm) silicate dust at temperatures above $\gtrsim 160$ K.

Key words. Circumstellar matter – stars: pre-main sequence – protoplanetary disks – stars: individual (HD 100453, HD 34282) – planet-disk interactions – stars: variables: T Tauri, Herbig Ae/Be

1. Introduction

Transitional disks have dust depleted gaps and inner holes in their dust distribution and form a special class of protoplanetary disks (Williams & Cieza 2011). The presence of gaps and inner holes may be indicators that planets are forming in the disks. To search for evidence of planet formation and characterize their physical and chemical conditions, the location and sizes of gaps in protoplanetary disks have to be investigated.

Transitional disks can be identified on the basis of their low near infrared excess (e.g. Calvet et al. 2005; Espaillat et al. 2007; Najita et al. 2007). Analysis of their spectral energy distribution (SED) may indicate that their inner regions are depleted of dust. However, modeling the radial disk structure by fitting only the SED is highly degenerate. Direct imaging of a protoplanetary disks is essential to derive the radial and azimuthal density structure. High spatial resolution observations of transitional disks reveal complex disk structures and can be used to study the interaction between gaps and proto-planets (e.g. van der Marel et al. 2013; Casassus et al. 2013; Quanz et al. 2013). Characterizing the connection between the radial structure and the SED is thus important to gain insight in the role of planet formation in the evolution of protoplanetary disks.

Herbig Ae/Be stars are intermediate mass stars with circumstellar disks (e.g. Natta et al. 2007). The SEDs of Herbig Ae/Be stars fall apart into two groups (Meeus et al. 2001). Group I, with strong excess at mid- to far-infrared wavelengths, and group II, without strong excess at mid- to far-infrared, but with a remarkable similarity in spectral shape. A first interpretation for the evolutionary link between these groups was proposed by Dullemond & Dominik (2004, 2005). These authors suggested that grain growth and settling cause the mid- to far-infrared excess to decrease. It was proposed that in this scenario, the disk structure evolves from flaring (group I) to flat (group II). However, recent studies indicate that almost all group I objects have large gaps (Grady et al. 2005; Honda et al. 2012; Maaskant et al. 2013). This implies that it is unlikely that group I sources with large gaps can evolve to group II disks, where no large gaps are found. To solve this issue, Maaskant et al. (2013) suggested that both groups evolve from a primordial continuous flaring disk, but may follow different pathways. The disks of group I objects are flaring/transitional due to the formation of large gaps. The disks of group II objects are self-shadowed because grain growth and vertical settling have flattened the outer disk.

In this paper, we investigate spatially resolved direct imaging mid-infrared observations of two protoplanetary disks presented in Mariñas et al. (2011). As these images are most sensitive to thermal emission of micron sized grains, they are suitable to study the radial density structure of transitional disks with large dust depleted gaps. To derive the properties of the disk, we perform a similar analysis of Q-band images as carried out in Maaskant et al. (2013).

The content of this paper is outlined in the following way. In Section 2, we introduce the Herbig stars HD 100453 and HD 34282. In Section 3 we discuss the Q-band observations and photometric properties of our sample. Section 4 describes the

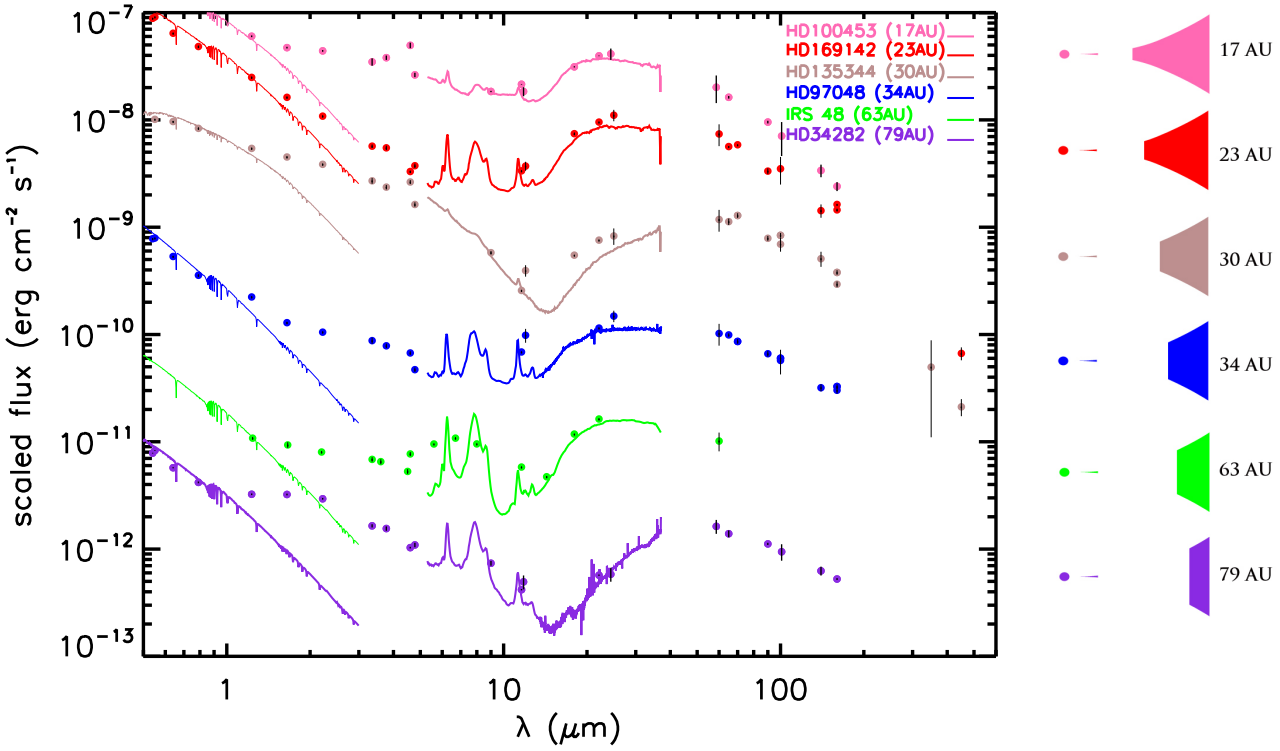

Fig. 1. The SEDs of group Ib Herbig Ae/Be stars in the sample of Maaskant et al. (2014). There is a great similarity in the shape of the SEDs. The fluxes are scaled so that the objects are sorted by gap size, with the smallest gap radius on top and the largest gap radius on the bottom. The flux scaling factors for the objects from top to bottom are respectively 10, 5, 1, 0.03, 0.003, 0.003.

radiative transfer code MCMax and the dust model. In section 5 we derive the properties of the disk structures and constrain the radii of the inner edges of the outer disks. The discussion and conclusions are given in Sections 6 and 7.

2. The sample

The Herbig Ae/Be objects HD 100453 and HD 34282 are studied in this paper. In this section, we present a brief summary. The SEDs of HD 100453 and HD 34282 are characterized by a strong excess of MIR emission at $\sim$ 15 – 40 μm (Figure 1). HD 100453 may show a very weak sign of amorphous silicate features, while in HD 34282 they are totally absent. The spectra of HD 100453 and HD 34282 show PAH emission bands. Their $I_{6.2}/I_{11.3}$ feature ratios are respectively 2.25 and 1.82 and relatively high, possibly indicating optically thin gas flows through the disk gaps (Maaskant et al. 2014).

2.1. HD 100453

HD 100453 is thought to be in transition between a gas rich protoplanetary disk and a gas poor debris disk (Collins et al. 2009). Observations of spatially resolved Q-band imaging (Mariñas et al. 2011), the SED and the absence of the silicate feature are indications of a gap Maaskant et al. (2013). HD 100453 has a close M-type companion (projected distance of 120 AU), the connection of the companion with the disk structure is not well understood (Collins et al. 2009). The stellar properties are taken from Meeus et al. (2001), where a the distance 114^{+11}_{-9} pc is adopted based on Hipparcos measurements.

parameter	unit	HD 100453	HD 34282
R.A.	(J2000)	11:33:05.58	05:16:00.48
Dec.	(J2000)	-54:19:28.5	-09:48:35.4
T	K	7400	8625
L_*	$L_\odot$	10.0	13.6
d	pc	114^{+11}_{-9}	348^{+129}_{-77} pc
M_*	$M_\odot$	1.66	1.59

Table 1. Stellar parameters used in this study. The parameters of HD 100453 are taken from van den Ancker et al. (1998) and the stellar properties of HD 34282 are taken from Merín et al. (2004).

2.2. HD 34282

Acke et al. (2009) already suggested that the disk around HD 34282 has a large opacity gap based on the near IR excess and far IR color. Rotational J=3-2 CO emission (Greaves et al. 2000), but no rovibrational CO emission (Carmona et al. 2005) was detected in this source, which is consistent with an evacuated inner disk but gas rich outer disk. We adopt the stellar properties derived by Merín et al. (2004) putting this source at a distance of 348^{+129}_{-77} pc.

3. Observations

We collect data of HD 100453 and HD 34282 which we use for the analysis of this paper. The SEDs and Q-band radial brightness profiles (RBPs) are shown in Figures 2 and 3. In addition, we compare these two objects to other similar transitional disks of the sample of Herbig stars presented in Maaskant et al. (2013, 2014).

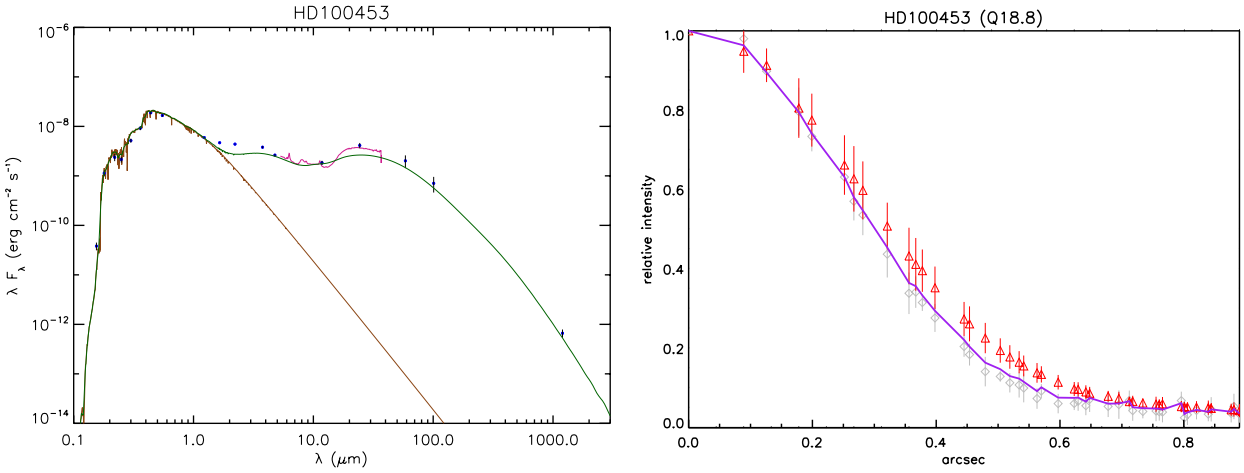

Fig. 2. This figure presents the model for HD 100453 where a continuous disk is assumed (i.e. no gap). The model fit to the SED seems reasonable, although the detailed spectral shape at ∼20 μm is not well fitted, though, the convolved model image does not fit the observed radial brightness profile. **Left:** The solid brown lines show the stellar Kurucz models. The solid red lines show the Spitzer/IRS spectra. The blue dots represent the observed photometry. The solid green lines show the total fluxes. **Right:** azimuthally averaged radial brightness profiles of the Q-band relative to the maximum flux for HD 100453 (top) and HD 34282 (bottom). The central wavelengths of these images are 18.8μm for both of the stars. The grey diamonds indicate the PSF of the calibration star. The red triangles show the observation of the science targets. The error bars indicate the one sigma error on the azimuthally averaged radial brightness profiles. The solid purple line shows our best-fit model.

3.1. Data

Q-band mid-Infrared images of HD 100453 and HD 34282 with effective central wavelengths of 18.2 μm are adopted from Mariñas et al. (2011). These observations are taken with the T-ReCS detector on Gemini south telescope on UT 6th Feb, 2006 and 4th Dec, 2003 respectively. The reduction of the T-ReCS imaging data have been done with IRAF MIDIR package provided by Gemini. The pixel scale of the data is 0.089 arcsec/px. The observations of the disks around the Herbig stars HD 100453 and HD 34282 are resolved with respect to their point spread functions derived from observations of the calibration stars with FWHM sizes of respectively 0.23 ± 0.06″ and 0.34 ± 0.07″. For all observational details we refer to Mariñas et al. (2011).

The MIR spectra of the disks are obtained by the Spitzer/IRS telescope and are adopted from Juhász et al. (2010) and Acke et al. (2010). The photometric data is taken from the literature and shown in Tables 2 and 3. The central star is described by a Kurucz model with the stellar parameters presented in table 1. Figures 2 and 3 show the SEDs and RBPs. The inclination of the disks are not well constrained, therefore we have adopted inclinations of 45 degrees for both sources.

3.2. The SEDs of transitional disks

The mid-IR parts of the SEDs of group Ib Herbig Ae/Be stars show similar shapes (see Figure 1). All objects show an emission bump at ∼20 μm and PAH features. In HD 100453, a weak signature of the amorphous 10 and 20 μm silicate features can be seen. All other sources show no sign of amorphous silicate features. In the next section we will characterise the gaps in the disks of HD 100453 and HD 34282 and confirm that the weakness of the silicate feature is connected to the presence of large gaps. The detailed shape of the SED is degenerate as it depends on parameters such as temperature and density structure as well as the composition of the disk. Though, the 'bump' in the the SED at MIR wavelengths for these objects is an indicator of large gaps in the disks of group Ib Herbig Ae/Be stars. Radiative transfer modeling of the Q-band is needed to constrain the radii of the inner edges of the outer disks of HD 100453 and HD 34282.

Table 2. Photometric data HD 100453 (not corrected for extinction) used in this study

band ID	λ [μm]	F_ν [Jansky]	reference
IUE 15	0.15	0.002 ± 0.000	a
IUE 18	0.18	0.066 ± 0.001	a
IUE 22	0.22	0.167 ± 0.003	a
IUE 25	0.25	0.172 ± 0.003	a
IUE 30	0.30	0.503 ± 0.009	a
Johnson U	0.36	1.079 ± 0.025	b
Johnson B	0.44	2.717 ± 0.036	b
Johnson V	0.55	2.993 ± 0.028	b
Near-IR J	1.23	2.433 ± 0.045	b
Near-IR H	1.65	2.571 ± 0.048	b
Near-IR K	2.22	3.237 ± 0.060	b
WISE 1	3.35	3.868 ± 0.304	c
Near-IR L	3.77	4.766 ± 0.225	b
WISE 2	4.60	7.582 ± 0.441	c
Near-IR M	4.78	4.180 ± 0.197	b
AKARI S09	9.00	5.518 ± 0.077	d
WISE 3	11.60	8.308 ± 0.053	c
IRAS 12	11.80	7.234 ± 0.698	e
AKARI S18	18.00	18.740 ± 0.248	d
WISE 4	22.10	29.131 ± 0.187	c
IRAS 25	25.00	33.533 ± 4.092	e
IRAS 60	60.00	39.379 ± 11.351	e
AKARI S65	65.00	35.230 ± 0.965	d
AKARI S90	90.00	28.650 ± 0.812	d
IRAS 100	100.00	23.822 ± 8.313	e
AKARI S140	140.00	15.770 ± 2.120	d
AKARI S160	160.00	12.810 ± 1.220	d
SIMBA 1.2 mm	1200.00	0.265 ± 0.021	f

References: **a)** IUE archival data **b)** Malfait et al. 1998 **c)** WISE All-Sky Data Release **d)** AKARI/IRC mid-IR all-sky Survey **e)** IRAS Point-source catalogue **f)** Meeus et al. 2003

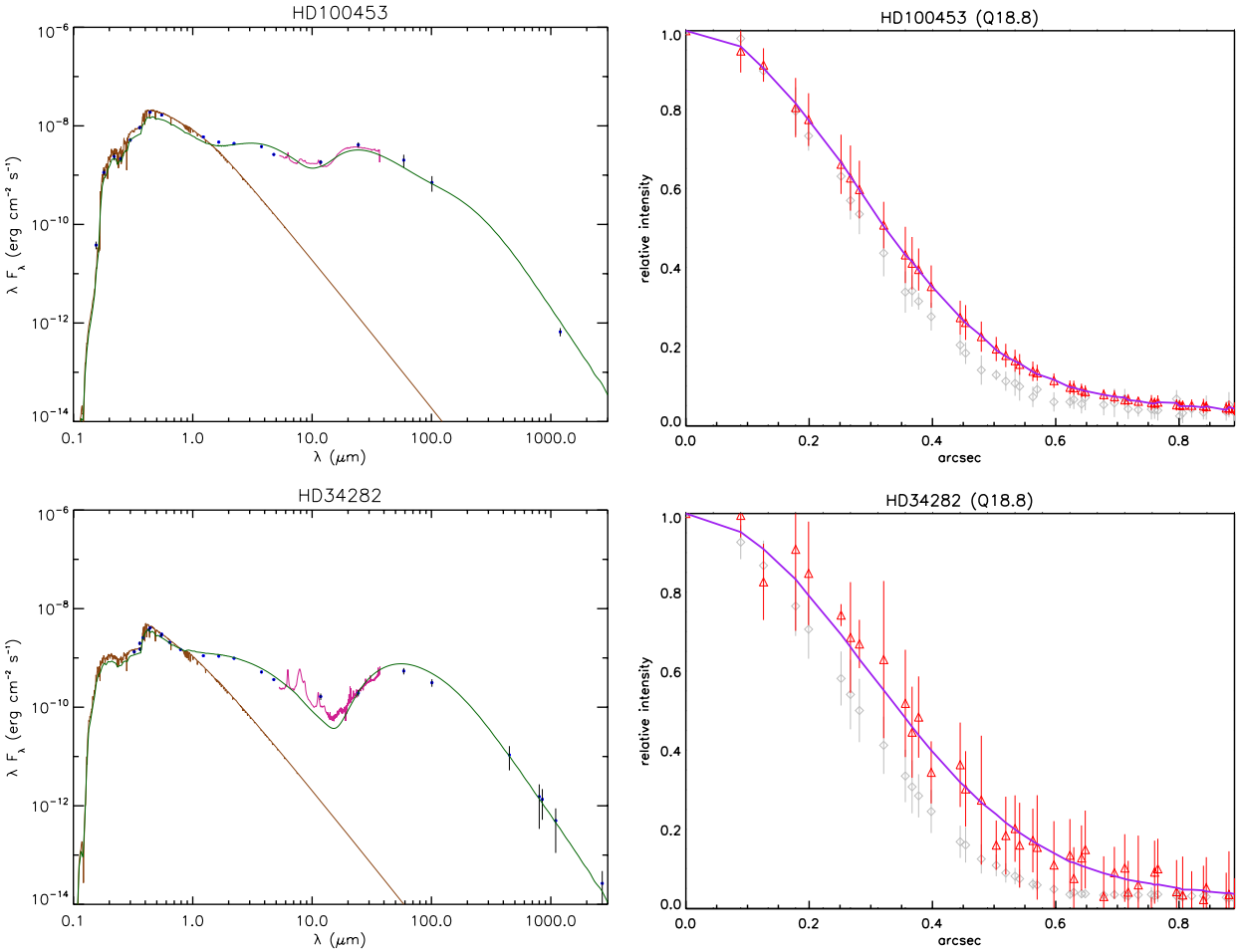

Fig. 3. The SED (right) and Q-band (left) of the best fit models for HD 100453 (top) and HD 34282 (bottom). See the caption of Figure 2 for a description of the lines and symbols shown in this figure.

4. Modeling

In this section we introduce the radiative transfer code MCMax and the dust model. We discuss the modeling approach and outline the parameters that we study in this paper.

4.1. Radiative transfer code MCMax

For the modelling of the disks, we use MCMax dust modelling and radiative transfer tool (Min et al. 2009). MCMax performs radiative transfer using a Mont Carlo recipe outlined by Bjorkman & Wood (2001). It solves the temperature structure and density structure assuming a 2-D geometry. It is used for modelling of circumstellar material including high optical depth regions. Our aim is to fit models to the observed Q-band images and SEDs of our sample stars to derive the disk structure. Therefore, we azimuthally average the Q-band brightness profiles and evaluate the radial extent of the disk emission. An extensive description of the modeling approach can be found in Maaskant et al. (2013).

4.2. Dust model

The composition of the grains in the disk are 20 % carbon and 80 % silicates. The standard dust composition with reference to the optical constants, is 32% $MgSiO_3$ (Dorschner et al. 1995), 34% Mg_2SiO_4 (Henning & Stognienko 1996), 12% $MgFeSiO_4$ (Dorschner et al. 1995), 2% $NaAlSi_2O_6$ (Mutschke et al. 1998), 20% C (Preibisch et al. 1993). The shape of our particles is irregular and approximated using a distribution of hollow spheres (DHS, Min et al. 2005) using a vacuum fraction of 0.7.

5. Results

In this section we describe the disk parameters that we constrain by fitting the size of the Q-band image. Thereafter we present the best fitting radiative transfer models to the Q-band sizes and the SEDs of HD 100453 and HD 34282.

5.1. Constraining the gap size

It has been shown by Maaskant et al. (2013) that the disk parameter that is constrained by fitting the Q-band size is the inner radius of the outer disk (i.e. the location of the wall). We perform a modeling study in Appendix A to study the effect to the SED of the inner and outer radii of the outer disk, the mass of the outer disk and the grain properties. We confirm that only the inner radius of the outer disk substantially effects the Q-band size. In the remainder of this section we fit the Q-band and SED of HD 100453 and HD 34282.

To fit the SED as well as the Q-band size we follow the fitting procedure as outlined in Maaskant et al. (2013). We summarize the procedure briefly here. As a first step, we start with a disk

Table 3. Photometric data HD 34282 (not corrected for extinction) used in this study

band ID	λ [μm]	F_ν [Jansky]	reference
Walraven W	0.32	0.095 ± 0.002	a
Johnson U	0.36	0.162 ± 0.004	b
Walraven U	0.36	0.125 ± 0.002	a
Walraven L	0.38	0.231 ± 0.006	a
Walraven B	0.43	0.392 ± 0.005	a
Johnson B	0.44	0.443 ± 0.006	b
Walraven V	0.54	0.408 ± 0.004	a
Johnson V	0.55	0.441 ± 0.004	b
Cousins R	0.64	0.364 ± 0.005	a
Cousins I	0.79	0.339 ± 0.007	a
Near-IR J	1.23	0.427 ± 0.008	b
Near-IR H	1.65	0.578 ± 0.011	b
Near-IR K	2.22	0.715 ± 0.013	b
WISE 1	3.35	0.607 ± 0.021	c
Near-IR L	3.77	0.646 ± 0.030	b
WISE 2	4.60	0.524 ± 0.009	c
Near-IR M	4.78	0.577 ± 0.027	b
AKARI S09	9.00	0.736 ± 0.038	d
WISE 3	11.60	0.538 ± 0.008	c
IRAS 12	11.80	0.647 ± 0.096	e
WISE 4	22.10	1.401 ± 0.020	c
IRAS 25	25.00	1.577 ± 0.234	e
IRAS 60	60.00	10.604 ± 1.571	e
AKARI S65	65.00	10.040 ± 0.726	d
AKARI S90	90.00	11.170 ± 0.261	d
IRAS 100	100.00	10.584 ± 1.851	e
AKARI S140	140.00	9.745 ± 0.932	d
AKARI S160	160.00	9.353 ± 0.186	d
450 micron	450.00	1.611 ± 0.826	b
800 micron	800.00	0.409 ± 0.318	b
1100 micron	1100.00	0.183 ± 0.142	b
PDB 1.3	1300.00	0.100 ± 0.023	g
2600 micron	2600.00	0.024 ± 0.019	f
PDB 3.2	3200.00	0.0055 ± 0.001	g

References: **a)** de Winter et al. 2001 **b)** Sylvester et al. 1996 **c)** WISE All-Sky Data Release **d)** AKARI/IRC mid-IR all-sky Survey **e)** IRAS Point-source catalogue **f)** Mannings & Sargent 2000 **g)** Natta et al. 2004

which has a continuous density profile. We assume that the disk is in hydrostatic equilibrium and that the radial dependence of the surface density drops off proportional to a powerlaw of -1. We fit the far-Infrared (FIR) to mm photometry to a grain size powerlaw index of p between 3.0 and 4.0. If this does not fit the Q-band size, than we insert a gap in the disk. We decrease the surface density in the gap by 15 orders of magnitude. This will result in a "wall" structure at the inner edge of the outer disk. Now we choose the radius of the inner edge of the outer disk, so that the convolved model image fits the observed Q-band image size. Then, we fit the emission in the NIR by including an optically thick inner disk. This will increase the flux in the NIR but casts a shadow on the outer disk and therefore reduces the flux at MIR and FIR wavelengths. In the case that an optically thick inner disk does not produce enough NIR flux or casts too much shadow on the outer disk, we add or replace an optically thin inner spherical halo to fit the NIR flux. As a final step, we choose the minimum size (between 0.1 μm and 1 μm) of the grains in the disk to fit the flux in the MIR and FIR to the SED.

5.2. Best-fit model HD 100453

We first explore models without a gap in the disk. This seems to fit the SED reasonably well, though it always fails to fit the size of the Q-band image (see Figure 2, right panel). We find that this is because for a continuous disk, the disk surface which is emitting in the Q-band is much closer to the star (i.e. $\lesssim$ 10 AU). Therefore, the model Q-band image is barely resolved with respect to the PSF (Figure 2). We can only fit the size of the Q-band by including a gap in the disk.

The model that gives us the best-fitted SED (Figure 3-left) and radial brightness profile (Figure 3-right) has a gap in the disk. We find that the inner edge of the outer disk has a very high surface brightness and dominates the emission in the Q-band. For this reason, the Q-band size is very sensitive for the location of the inner edge of the outer disk. We constrain its location at 17^{+2}_{-2} AU. The error is dominated by the uncertainty in the distance. As can be seen in Figure 3-right, the convolved image that is modelled using these input parameters fits well with this observation. The average temperature of the inner edge (17 – 20 AU) of the outer disk is ~160 K.

The structure of the inner disk is poorly constrained by our data. Therefore we have modelled the inner circumstellar region by spherical halos which are optically thin, but geometrically high. To fit the near-infrared (NIR) emission we adopt a halo from 0.1 to 1.7 AU with a mass of 0.15×10^{-9} $M_\odot$. As there are many uncertainties in the structure of the inner disk (e.g. Dullemond & Monnier 2010), we only use the halo in our model in order to reproduce the amount of produced NIR emission from the disk. To account for the absence of silicate features at 10 and 20 μm, we assume a dust specie in the halo which does not show any features. We adopt 100% amorphous carbon, but alternatively, larger silicate grains or metallic iron may yield similar results.

The values of the best-fit parameters are listed in Table 4 and also compared with the values obtained for four other Herbig star by Maaskant et al. (2013).

5.3. Best-fit model HD 34282

For the the Herbig star HD 34282, we follow the same procedure as HD 100453. We find that we can not find a fit to the SED and Q-band size by using a disk with a continuous density structure. Therefore we adopt a gap in the disk. The best SED fit can be seen in Figure 3-right and its radial brightness profile is shown in Figure 3-right. The location of the inner radius of the outer disk is constrained to 79^{+31}_{-17} AU. Although the signal to noise of the Q-band observation is of worse than that of HD 100453, the error is still dominated by the uncertainty in the distance.

The model of the disk includes a halo that is extended from 0.02 to 1.3 AU and has a mass of 2.4×10^{-11} $M_\odot$. The dust grains in the halo are made of carbon and they have the size of 0.5 μm to 1 mm with an size distribution power law of -3.5. The mass of the outer disk is considered to be 0.83×10^{-4} $M_\odot$.

5.4. Summary

By using radiative transfer models, we have studied the Q-band sizes and SEDs of HD 100453 and HD 34282. We fail to find solutions with a continuous density structure. Thus we find that is is required to include large gaps in the disk to simultaneously fit the Q-band size and SED. The inner edge of the outer disks of HD 100453 and HD 34282 are respectively 17^{+2}_{-2} AU and 79^{+31}_{-17} AU.

6. Discussion

For HD 100453 and HD 34282, radii of the inner edges of the outer disks have been derived from the best-fit models. These values are in the same range as the wall radii of disks around

Object	M_{dust} $M_\odot$	M_{halo} $M_\odot$	$R_{innerdisk/halo}$ AU	R_{wall} AU	R_{out} AU	$a_{min} - a_{max}$	a_{pow}
HD100453	3.2×10^{-4}	0.15×10^{-9}	0.1-1.7	17^{+2}_{-2}	200	0.5 μm - 1mm	-3.5
HD 3428	6.1×10^{-4}	5.5×10^{-11}	0.05-1.3	79^{+31}_{-17}	900	0.5 μm - 1mm	-3.5
HD 97048	6.0×10^{-4}	...	0.3 - 2.5	34^{+4}_{-4}	500	0.5 μm - 1mm	-3.5
HD 169142	0.8×10^{-4}	0.31×10^{-12}	0.1- 0.2	23^{+4}_{-4}	235	0.5 μm - 1mm	-3.5
HD 135344 B	1.0×10^{-4}	0.47×10^{-12}	0.1- 0.3	30^{+4}_{-3}	200	1.0 μm - 1mm	-4.0
Oph IRS 48	3.0×10^{-5}	0.50×10^{-12}	0.1 -0.3	63^{+4}_{-4}	235	0.1 μm - 1mm	-4.0

Table 4. Best-fit model parameters and comparison to the previous values by Maaskant et al. 2013

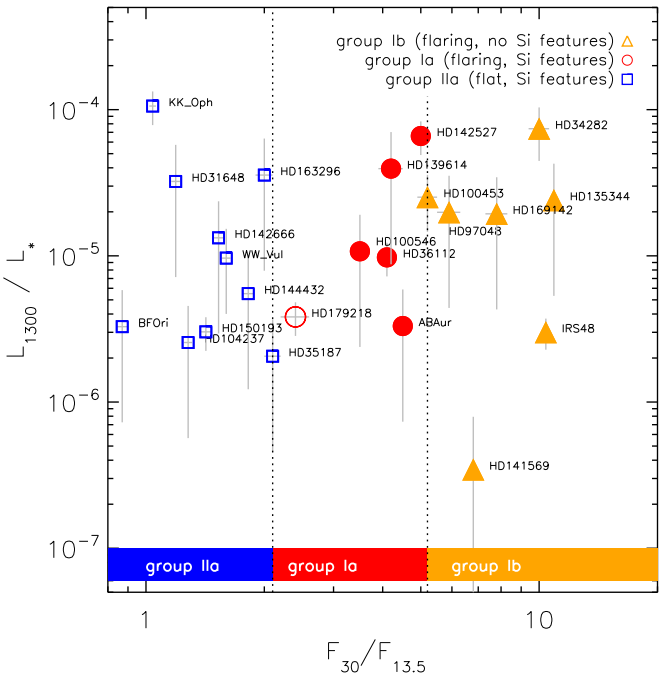

Fig. 4. The luminosities at 1.3 mm is compared to the flux ratio at 30.0 and 13.5 μm. The filled symbols indicate whether large gaps have been detected in the literature. The L_{1300}/L_* can be used as a proxy of the disk mass. We confirm the connection between the gap size and its location, with the $F_{30}/F_{13.5}$ ratio. All the objects in this diagram are taken from the sample of Maaskant et al. (2014).

other group Ib Herbig stars. We now discuss the implications of these results.

6.1. New Meeus group classification based on the $F_{30}/F_{13.5}$ continuum flux ratio

We compare the photometric properties of HD 100453 and HD 34282 to other Herbig stars. Figure 4 shows the color-magnitude and classification of a sample of Herbig stars. It shows luminosities at 1.3 mm compared to flux ratios at 30.0 and 13.5 μm for Herbig stars from the sample of Maaskant et al. (2014). As disks lose their mass during their evolution, they move down in this diagram. This diagram seems to indicate that there is no trend between group I and group II disks with regard to the disk mass. Previous studies (Acke et al. 2009; Maaskant et al. 2013, 2014) have indicated a strong correlation between the $F_{30}/F_{13.5}$ continuum flux ratio and the group classification based on (Meeus et al. 2001). The transitions between group Ia, Ib and group IIa may be more easily expressed by the the $F_{30}/F_{13.5}$ ratios. For flat sources with amorphous silicate features (group IIa) that implies $F_{30}/F_{13.5} \leqslant 2.1$. For transitional/flaring objects with amorphous silicate features (group Ia) we find $2.1 < F_{30}/F_{13.5} < 5.1$. The transitional/flaring objects which do not have silicate feature (group Ib) have $F_{30}/F_{13.5} \geqslant 5.1$. The Meeus groups are well separated by the new criteria based on the mid-infrared flux ratio 4.

6.2. Correlation between amorphous silicate emission, size of the gap and the $F_{30}/F_{13.5}$ ratio

Tansitional flaring disks which do show silicate emission are group Ia Herbig Ae/Be stars. The amorphous silicate features in these objects may originate in the inner edge of the outer disk. This may be the case for HD 100456 (e.g. Mulders et al. 2011) and HD 139614 (Matter et al. 2014), two transitional objects with the inner edge of the outer disk at respectively 13 and 5 AU. Alternatively, the amorphous silicate feature may originate in the inner disk. Examples are HD 142527 (Verhoeff et al. 2011), AB Aur (Honda et al. 2010) and HD 36112 (Isella et al. 2010). Also in these objects large gaps of several tens of AU's have been found. However, the inner disk may still contain a substantial amounts of small silicate grains producing the silicate features.

Group Ib Herbig Ae/Be stars do not show silicate emission features. Our study confirms that the weakness of silicate emission features is connected to the presence of large disk gaps in the critical temperature regime ($\gtrsim$160 K) responsible for emission of silicate features. HD 100453 has the smallest gap size in the sample of group Ib objects. Peculiarly, a closer look at the Spitzer/IRS spectrum of HD 100453 may show a tentative detection of very weak amorphous silicate features (Figure 1). Figure 4 shows that the $F_{30}/F_{13.5}$ ratio of HD100453 is on the border of a group Ia identification. We suggest that this is connected to the relatively small gap radius of 17 AU and thus higher temperature in the inner region of the outer disk. Our radiative transfer model of HD 100453 shows that the average temperature of the inner region of the outer disk (between 17 – 20 AU) is ~160 K. Because the inner edge of the outer disk is closer to the star, the temperature of the dust in the wall is higher than for HD 34282 and the other group Ib transitional disks studied in Maaskant et al. (2013). We can compare the temperature in the wall of HD 100453 to that of HD 100546 and HD 97048. HD 100546 is one of the best studied transitional disks which does show strong amorphous silicate features. Radiative transfer models presented in Mulders et al. (2011) show that the inner edge of the outer disk of HD 100546 is located at ~13 AU and has a temperature of ~200 K. For HD 97048, the typical temperature in the inner region of the outer disk (34 – 37 AU) is ~110 K (Maaskant et al. 2013). HD 97048 does not show any sign of amorphous silicate emission. From this comparison, we infer that the temperature transition from ~160 K to ~200 K in the inner edge of the outer disk is critical for the strong enhancement of the amorphous silicate features originating in the wall. Possibly this is connected

to the fact that grains of $\lesssim$160 K are icy and therefore grow to larger typical sizes (e.g. Sirono 2011; Okuzumi et al. 2012). The slow sublimation of ice in icy aggregates at $\sim$ 160 K, which are radially drifting inward in the disk, will lead to the formation of "pure" silicate aggregates which are thus more fragile and can readily fragment upon collision. In this scenario, an enhanced abundance of small fragmented silicate grains at temperatures of $\gtrsim$ 160 K, may contribute significantly to the amorphous silicate features.

6.3. Evolutionary link between transitional (flaring) and self-shadowed (flat) disks.

A key question in the study of protoplanetary disks is to determine the evolutionary link between gaps formation (group I) and grain growth and settling (group II). Disk gaps are found in an increasing number of group I Herbig stars and there is yet no evidence of large gaps in group II Herbig stars (Maaskant et al. 2013). Therefore, it is very unlikely that group I evolves to group II. There are now two possible evolutionary scenario's to understand the link between group I and II. First, as proposed by Maaskant et al. (2013), both groups may have evolved from a common ancestor (i.e., gapless flaring-disk structure). In transitional group I objects, gap formation has proceeded the collapse of the outer disk while grain growth and dust settling have flattened the outer disk in flat group II objects. Secondly, group II objects may be the precursors of group I objects. In that case, possibly planet formation is followed by the formation of a large gap that may produce a high vertical wall and stir up the dust in the outer disk.

7. Conclusions

We have used spatially resolved MIR observations and radiative transfer models. We fit the spectral energy distribution and the radial brightness profile of the Q-band images of the disks around two Herbig Ae/Be type Ib stars, HD 100453 and HD 34282. This work is compared to the results of Maaskant et al. (2013), where a similar analysis of four other Herbig stars, HD 97047, HD 169142, HD 135344 B and Oph IRS 48, is presented.

- We were not able to fit the spatially resolved Q-band imaging and SEDs considering a continuous disk (i.e. no gap). In contrast with a transitional disk consisting of a halo around the star, a gap and an hydrostatic outer disk, we successfully fit all the observations.
- Radiative transfer modelling constrains the inner radius of the outer disk at 17^{+2}_{-2} AU for HD 100453 and 79^{+31}_{-17} AU for HD 34282. This result confirms the conclusion by Maaskant et al. (2013) that group Ib Herbig Ae/Be stars are transitional disks with large gaps.
- The outer disk mass, surface density power law, and the opacity profile do not affect the Q-band size.
- We find no correlation between the halo masses, the disk masses and the sizes of the gaps in studied Herbig Ae/Be stars.
- The absence of the amorphous silicate emission in the spectra of these disks is consistent with the conclusions of Maaskant et al. (2013) that gaps in a critical temperature regime between $\sim$ 200 – 500 K cause the silicate feature to disappear.
- The temperature transition from ~160 K to ~200 K in the inner edge of the outer disk is critical for the strong enhancement of the amorphous silicate features originating in the wall

Acknowledgements. The authors thank Rens Waters for inspiring discussions which helped to improve the analysis in this paper. K.M. is supported by a grant from the Netherlands Research School for Astronomy (NOVA). Studies of interstellar chemistry at Leiden Observatory are supported through advanced-ERC grant 246976 from the European Research Council, through a grant by the Dutch Science Agency, NWO, as part of the Dutch Astrochemistry Network, and through the Spinoza premie from the Dutch Science Agency, NWO.

References

Acke, B., Bouwman, J., Juhász, A., et al. 2010, ApJ, 718, 558
Acke, B., Min, M., van den Ancker, M. E., et al. 2009, A&A, 502, L17
Bjorkman, J. E. & Wood, K. 2001, ApJ, 554, 615
Calvet, N., D'Alessio, P., Watson, D. M., et al. 2005, ApJ, 630, L185
Carmona, A., van den Ancker, M. E., Thi, W.-F., Goto, M., & Henning, T. 2005, A&A, 436, 977
Casassus, S., van der Plas, G., M, S. P., et al. 2013, Nature, 493, 191
Collins, K. A., Grady, C. A., Hamaguchi, K., et al. 2009, ApJ, 697, 557
de Winter, D., van den Ancker, M. E., Maira, A., et al. 2001, A&A, 380, 609
Dorschner, J., Begemann, B., Henning, T., Jaeger, C., & Mutschke, H. 1995, A&A, 300, 503
Dullemond, C. P. & Dominik, C. 2004, A&A, 421, 1075
Dullemond, C. P. & Dominik, C. 2005, A&A, 434, 971
Dullemond, C. P. & Monnier, J. D. 2010, ARA&A, 48, 205
Espaillat, C., Calvet, N., D'Alessio, P., et al. 2007, ApJ, 670, L135
Grady, C. A., Woodgate, B. E., Bowers, C. W., et al. 2005, ApJ, 630, 958
Greaves, J. S., Mannings, V., & Holland, W. S. 2000, Icarus, 143, 155
Henning, T. & Stognienko, R. 1996, A&A, 311, 291
Honda, M., Inoue, A. K., Okamoto, Y. K., et al. 2010, ApJ, 718, L199
Honda, M., Maaskant, K., Okamoto, Y. K., et al. 2012, ApJ, 752, 143
Isella, A., Natta, A., Wilner, D., Carpenter, J. M., & Testi, L. 2010, ApJ, 725, 1735
Juhász, A., Bouwman, J., Henning, T., et al. 2010, ApJ, 721, 431
Maaskant, K. M., Honda, M., Waters, L. B. F. M., et al. 2013, A&A, 555, A64
Maaskant, K. M., Min, M., Waters, L. B. F. M., & Tielens, A. G. G. M. 2014, ArXiv e-prints
Malfait, K., Bogaert, E., & Waelkens, C. 1998, A&A, 331, 211
Mannings, V. & Sargent, A. I. 2000, ApJ, 529, 391
Mariñas, N., Telesco, C. M., Fisher, R. S., & Packham, C. 2011, ApJ, 737, 57
Matter, A., Labadie, L., Kreplin, A., et al. 2014, A&A, 561, A26
Meeus, G., Bouwman, J., Dominik, C., Waters, L. B. F. M., & de Koter, A. 2003, A&A, 402, 767
Meeus, G., Waters, L. B. F. M., Bouwman, J., et al. 2001, A&A, 365, 476
Merín, B., Montesinos, B., Eiroa, C., et al. 2004, A&A, 419, 301
Min, M., Dullemond, C. P., Dominik, C., de Koter, A., & Hovenier, J. W. 2009, A&A, 497, 155
Min, M., Hovenier, J. W., & de Koter, A. 2005, A&A, 432, 909
Mulders, G. D., Waters, L. B. F. M., Dominik, C., et al. 2011, A&A, 531, A93
Mutschke, H., Begemann, B., Dorschner, J., et al. 1998, A&A, 333, 188
Najita, J. R., Strom, S. E., & Muzerolle, J. 2007, MNRAS, 378, 369
Natta, A., Testi, L., Calvet, N., et al. 2007, Protostars and Planets V, 767
Natta, A., Testi, L., Neri, R., Shepherd, D. S., & Wilner, D. J. 2004, A&A, 416, 179
Okuzumi, S., Tanaka, H., Kobayashi, H., & Wada, K. 2012, ApJ, 752, 106
Preibisch, T., Ossenkopf, V., Yorke, H. W., & Henning, T. 1993, A&A, 279, 577
Quanz, S. P., Avenhaus, H., Buenzli, E., et al. 2013, ArXiv e-prints
Sirono, S.-i. 2011, ApJ, 735, 131
Sylvester, R. J., Skinner, C. J., Barlow, M. J., & Mannings, V. 1996, MNRAS, 279, 915
van den Ancker, M. E., de Winter, D., & Tjin A Djie, H. R. E. 1998, A&A, 330, 145
van der Marel, N., van Dishoeck, E. F., Bruderer, S., et al. 2013, Science, 340, 1199
Verhoeff, A. P., Min, M., Pantin, E., et al. 2011, A&A, 528, A91
Williams, J. P. & Cieza, L. A. 2011, ARA&A, 49, 67

Appendix A: parameter study

Figure A.1 shows the results of a small parameter study to illustrate the degeneracy of SED modeling. HD 100453 is shown on the left and HD 34282 is shown on the right.

The top left plot in Figure A.1 show the result of modelling different values for the inner radius of the outer disk (the wall radius). This value affects the MIR of the SED where the emission comes from the wall and the temperature is about ∼100-160 K. The gap size with the value of 17 AU fits the observed SEDs very well. This indicates a presence of a gap in between the halo and the outer disk. The exact size of this gap cannot be understood from modeling the SED alone, but must include fitting the size of the Qband image. The SED is degenerate because the structure of the inner halo (i.e. the optical depth, and scaleheigth), as well as the grain composition in the outer disk are not well known. As we will see, these parameters have a great influence on the SED as well.

The top right plot in Figure A.1, shows a comparison of different disk radii. The outer radius is unknown and we try some values in the range of typical disk sizes and we find that a disk size with radius of 200 AU fits better the SED better. However, the changes of this value do not have a significant effect on the outcome of the modelling and therefore, it is not easy to estimate the size of the outer radius of the disk.

The bottom left plot in Figure A.1 show variations in the dust mass. Higher mass means more material in the disk and therefore this would increase the thermal emission from the disk in the far-IR regions. Dust mass mainly affects the mm part of the SED. When the dust mass is taken to be lower than the best-fit value, the mm flux tends to shifts below the observation and when the mass is higher than the best fit, the mm flux shifts above the observation.

The bottom right plot in Figure A.1 shows the result for different opacity profiles (i.e. different grain sizes and power law indices). The best-fit consists of grain size distribution of 0.5 μm to 1 mm with the power law index of -3.5. The change in this parameter affects the temperature and luminosity of the halo and the location of the wall of the outer disk. This is especially noticeable in the NIR part of the SEDs. The red lines show the models with the highest abundance of small grains. Smaller grains have higher opacities, this means that more stellar radiation is absorbed the close to the star. Therefore the emission from the halo increases, but the stellar radiation decreases due to the higher optical depth. The other grain size populations show similar behaviours.

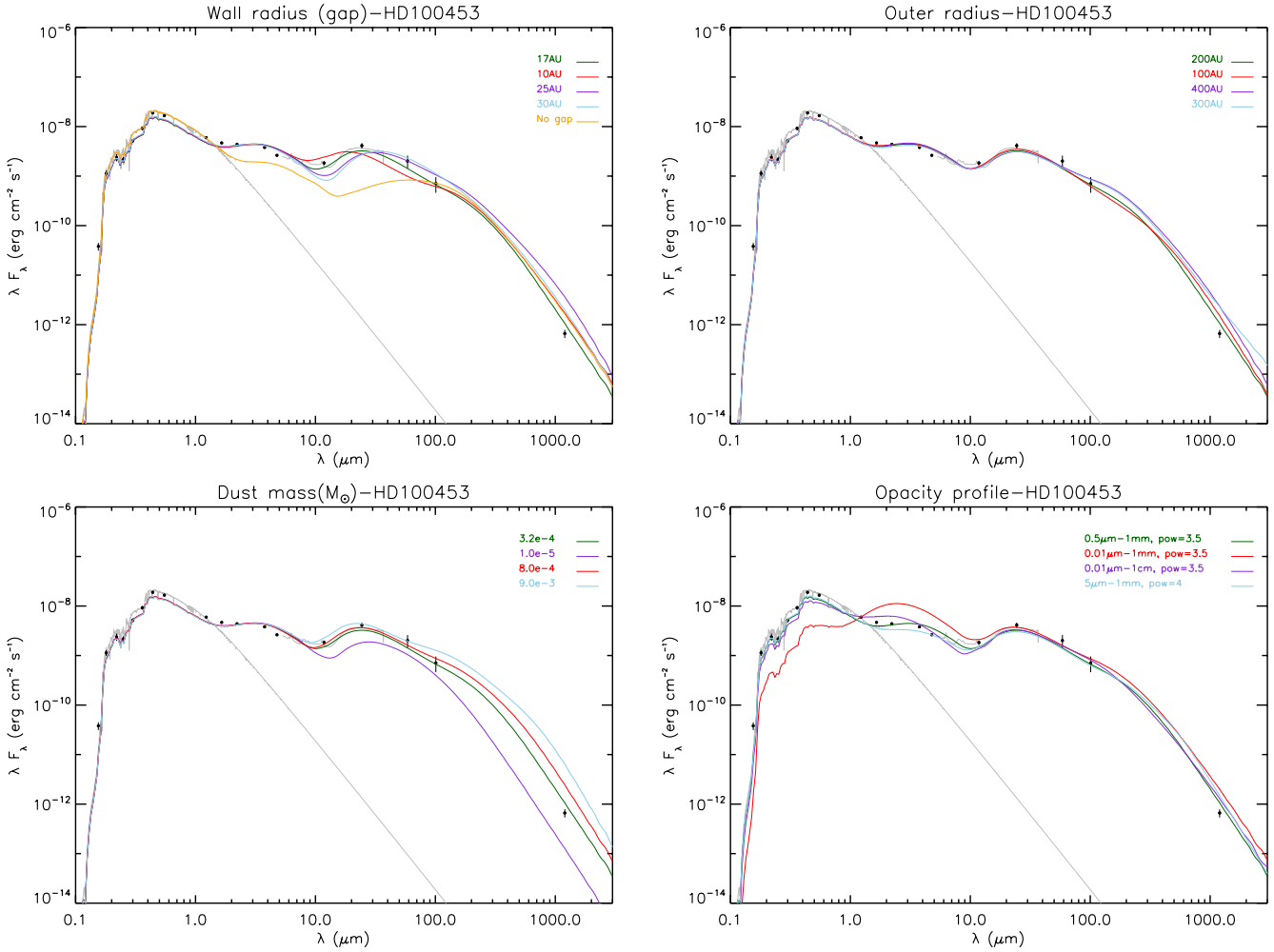

Fig. A.1. Variations around the best-fit values for HD 100453. Top left: different gap sizes. Top right: different radii of outer disk. Bottom left: different total disk masses. Bottom right: different minimum and maximum grain sizes and power-laws of the grain size distribution.